IEEE Access
Multidisciplinary ⋮ Rapid Review ⋮ Open Access Journal

Received August 10, 2021, accepted September 7, 2021, date of publication September 10, 2021,
date of current version September 28, 2021.

Digital Object Identifier 10.1109/ACCESS.2021.3111967

Transient Stability Improvement by Generator Tripping and Real-Time Instability Prediction Based on Local Measurements

SYLWESTER ROBAK, (Member, IEEE), JAN MACHOWSKI, (Member, IEEE), MATEUSZ M. SKWARSKI, AND ADAM SMOLARCZYK
Faculty of Electrical Engineering, Warsaw University of Technology, 00-661 Warsaw, Poland
Corresponding author: Sylwester Robak (sylwester.robak@ien.pw.edu.pl)

This work was supported by the ENERGYTECH-1 Project by Warsaw University of Technology through the Program Excellence Initiative: Research University (ID-UB).

ABSTRACT Special protection systems based on generator tripping are implemented to protect power systems against the loss of synchronism following extreme contingency events. Such a countermeasure is particularly effective when the circuit breakers of the tripped generators are opened soon after the fault is cleared. This paper presents the new method that enables quick real-time predictions of transient instability and the number of generators that must be tripped. The proposed method uses only local measurements and is based on the quick prediction of the magnitude of the power-angle characteristic. The proposed method has been validated by simulation tests performed for a large-scale real power system and detailed models of power system elements.

INDEX TERMS Power system transient stability, real-time instability prediction, generator tripping, special protection scheme.

I. INTRODUCTION

Contingency events in power systems are classified into two categories: planning contingency events (subdivided into credible and less credible ones) and extreme contingency events [1], [2]. For all planning contingency events, all rules of the performance standard (stability being among them) must be met without special protections and without any exceptions.

Generator tripping is a countermeasure to prevent the power system from losing synchronism [1], [3]–[5]. It is also used for alleviating overloads in transmission networks [6], [7] which may occur after fault clearance. Generator tripping has two drawbacks: (i) it causes power imbalance which must be corrected by an automatic generation control (AGC) and (ii) it can increase shaft fatigue. Therefore, the planning criteria restrict the use of generator tripping [2], [8] only to extreme (rare) contingency events. Transmission system operators also use generator tripping temporarily to limit the risk of blackouts during transitional periods when expansion of the transmission network is behind schedule and does not match growing generation power.

Automatic systems detecting the oncoming instability and undertaking corrective measures (such as generator tripping) are called special protection schemes (SPS) [9].

In the SPSs of the past and some modern ones used today generator tripping is activated using look-up tables and a preprogrammed off-line logic based on the multivariant off-line stability analysis [10]–[12]. The analysis and logic should consider several data classes such as network topology, setpoint of the generating units, fault type, fault location, and clearing time. The SPS described in [10] uses thirteen complementary algorithms based on local measurements. The threshold values occurring in these algorithms were determined using multivariant off-line power system simulations and scatter diagrams.

The important disadvantage of SPSs with preprogrammed logic is a limited scope for real-time adaptation. Due to the rigidity of logic in some states and/or for some faults the number of tripped generators may be either overestimated or underestimated. Fast instability prediction and real-time decision-making algorithms are the alternative to rigid logic. A recently published paper [13] shows an extensive review

The associate editor coordinating the review of this manuscript and approving it for publication was Siqi Bu.

of various methods used for instability prediction. However, most of them are intended for application in pole-slip protection, which is not addressed by this paper. Many publications have dealt with different instability prediction methods, however, they do not describe how such methods can be used for determining the number of generators that must be tripped.

The review of various preventive and emergency control techniques can be found in brochure [4] and papers [14], [15]. Publications [16] and [17] review instability prediction methods based on a wide-area measurement system (WAMS). Papers [18], [19] and [20] present interesting approaches based on WAMS using synchrophasors measured at generation nodes. Paper [21] describes a model-based predictive controller. Development of this type of SPSs seems to be very promising. A very recently published paper [22] describes experiments with applying deep learning models to instability prediction.

Over the last decades a lot of research has utilized the direct Lyapunov method for assessing transient stability and for stability-enhancing control. Publications [23], [24] and paper [25] present the brief review of such topics relating to a single-machine and infinite-busbar (SMIB) model. For such a simplified model, the direct Lyapunov method is equivalent to the well-established equal area method [1].

The method described in this paper also uses the equal area method, but the proposed approach is completely different. It uses only local measurements and does not require any time-consuming prediction of the post-fault system trajectory. Therefore, the proposed instability prediction method and the determination of the number of tripped generators are very quick.

II. MOTIVATION

Following extreme contingency events, generator tripping can effectively prevent transient instability of power systems only when the circuit breakers of generators are opened soon after the fault is cleared. Any delay increases the number of generators that must be tripped to preserve the synchronism of the remaining generators [1], [26]. At the same time, any delay in SPS operation increases power imbalance in the system and possible consequences such as decreased frequency and activation of load shedding. Therefore, early detection of instability is crucial when generator tripping is used to prevent the loss of synchronism.

The above fact has motivated the authors of this paper to develop a new instability prediction method and a new method to determine the number of generators to be tripped.

The proposed method is completely different from other instability prediction methods. While other available methods are based on the prediction of changes in power angle and speed deviation, the proposed decision-making method is based on the prediction of a single parameter which is the magnitude of the power-angle characteristic. Such an approach enables to predict instability very quickly and to determine the number of generators to be tripped.

The proposed method has been developed for a simple power system model, but its validity has been confirmed by the simulation on a real large-scale power system.

III. SIMPLIFIED MODEL AND TRANSIENT STABILITY

A group of synchronous generators operating on the same busbar in the simplest way can be represented by the SMIB model. The circuit diagram of such a model is shown in Figure 1. $\underline{E}$ and X'_{d} shown in this figure represent the electromotive force and transient reactance respectively. X_{T} is the step-up transformer reactance and $X_{\mathrm{G}} = X'_{\mathrm{d}} + X_{\mathrm{T}}$. P, Q are the active and reactive power of the equivalent generating unit. $\underline{V}_{\mathrm{G}}$ is the generator terminal voltage. The remaining part of the system is represented by the voltage source $\underline{V} = \text{const}$ and the equivalent reactance X_{S}. The power angle δ is the difference between the phase angles of $\underline{E}$ and $\underline{V}$.

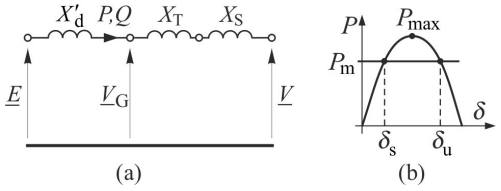

FIGURE 1. (a) Circuit diagram and (b) power-angle characteristic $P(\delta)$.

The rotor motion of the equivalent generator is described by the following differential equation:

$$M\frac{\mathrm{d}\Delta\omega}{\mathrm{d}t} = P_{\mathrm{m}} - P \tag{1}$$

where $M = T_{\mathrm{m}}S_{\mathrm{n}}/\omega_{\mathrm{s}} = 2HS_{\mathrm{n}}/\omega_{\mathrm{s}}$ is the inertia coefficient, $\Delta\omega = \mathrm{d}\delta/\mathrm{d}t$ is the speed deviation, P_{m} is the mechanical power, and P is the electrical power expressed by the following formula [1]:

$$P = \frac{EV}{X}\sin\delta = P_{\max}\sin\delta \tag{2}$$

where $X = X_{\mathrm{G}} + X_{\mathrm{S}}$ and $P_{\max} = EV/X$ is the magnitude of the power-angle characteristic $P(\delta)$ shown in Figure 1b.

The system described by equations (1) and (2) is nonlinear and therefore its transient stability depends on the type of fault and its duration and the electrical distance from the generator.

At the moment t_{c} (immediately after the fault clearance), the first-swing instability can be predicted by using the equal area criterion, which is equivalent to the direct Lyapunov method [1]. The system is stable if in the post-fault state the acceleration area A_{a} (proportional to the surplus of the kinetic energy released by the fault) is smaller than the available deceleration area A_{d} (proportional to the maximal work that the system can perform to preserve the synchronism).

IV. PREDICTION OF TRANSIENT INSTABILITY

The above stability conditions indicate that the magnitude of the power-angle characteristic $P_{\max}$ is a key parameter. Its prediction soon after the fault clearance enables predicting the instability of the power system and the number of generators that must be tripped to preserve the synchronism.

A. PREDICTION OF P_{max}

It is worth emphasizing that in the SMIB model (Fig. 1) the equivalent reactance X_S and voltage $\underline{V}$ generally have different values for pre-fault, fault, and post-fault states. Therefore, for each of these states the values of $P_{max} = EV/X$ vary considerably. This has been described in book [1] (Chapter 6.1) in detail. The abovementioned equal area criterion and direct Lyapunov method allow predicting instability immediately after the fault clearance. Thus, the following considerations apply to the post-fault state, for which X_S and $\underline{V}$ are fixed and can be treated as constant.

From equation (2), the following can be obtained:

$$(P_{max} \sin\delta)^2 = P^2 \tag{3}$$

The rate of change of the active power during power swings after the fault clearance is equal to the time derivative:

$$\frac{dP}{dt} = \frac{\partial P}{\partial \delta} \cdot \Delta\omega + \frac{\partial P}{\partial E} \cdot \frac{dE}{dt} \tag{4}$$

where $\Delta\omega = d\delta/dt$ is the speed deviation and

$$\frac{\partial P}{\partial \delta} = P_{max} \cos\delta; \quad \frac{\partial P}{\partial E} = \frac{V}{X} \sin\delta = \frac{P}{E} \tag{5}$$

Substituting equations (5) into equation (4) gives:

$$\frac{dP}{dt} = P_{max} \cos\delta \cdot \Delta\omega + \frac{P}{E} \cdot \frac{dE}{dt} \tag{6}$$

and hence:

$$(P_{max} \cos\delta)^2 = \left[\frac{dP}{dt} - \frac{P}{E} \cdot \frac{dE}{dt}\right]^2 \cdot \frac{1}{(\Delta\omega)^2} \tag{7}$$

The sum of the squares of sine and cosine is equal to 1 and therefore from the sum of equations (3) and (7) the following result can be obtained:

$$P_{max} = \sqrt{P^2 + \left(\frac{dP}{dt} - \frac{P}{E} \cdot \frac{dE}{dt}\right)^2 \cdot \frac{1}{(\Delta\omega)^2}} \tag{8}$$

At each moment of the transient state, the electromotive force E may be calculated based on the voltage drop across the transient generator reactance:

$$\underline{E} = \underline{V}_G + \frac{X'_d Q}{V_G} + j\frac{X'_d P}{V_G} \tag{9}$$

where j is the angular shift by $\pi/2$. Hence:

$$E = \sqrt{\left(V_G + \frac{X'_d Q}{V_G}\right)^2 + \left(\frac{X'_d P}{V_G}\right)^2} \tag{10}$$

where V_G and P, Q are the terminal voltage and the active and reactive generator power respectively.

The mathematical operations in equation (8) are not feasible if $\Delta\omega = 0$. However, this is not a problem for the prediction because soon after the fault clearance the speed deviation is always positive, $\Delta\omega > 0$.

B. TRANSIENT STABILITY CONDITION

It is assumed that at the moment t_c, immediately after the fault clearance, the speed deviation $\Delta\omega_c$ is known, while the surplus of kinetic energy equal to the acceleration area A_a is calculated by the following formula:

$$A_a = \frac{1}{2} M \cdot \Delta\omega_c^2 \tag{11}$$

The available deceleration area can be determined as the integral of the difference in the power-angle characteristic $P(\delta)$ and mechanical power P_m from angle δ_c to unstable equilibrium point δ_u:

$$\begin{aligned} A_d &= \int_{\delta_c}^{\delta_u} P_{max} \sin\delta d\delta - P_m \cdot (\delta_u - \delta_c) \\ &= P_{max}(-\cos\delta_u + \cos\delta_c) - P_m(\delta_u - \delta_c) \end{aligned} \tag{12}$$

where δ_c and P_c are the power angle and active power of the generator at moment t_c. The system is stable (i.e. synchronism is preserved) if the following stability condition is met:

$$A_d > A_a \tag{13}$$

In such a case, the transient stability margin

$$K = \frac{A_d - A_a}{A_d} \cdot 100\% \tag{14}$$

is positive. If $A_d < A_a$, the system is unstable and the margin (14) is negative.

Generally, all possible post-fault states (i.e. states after the fault clearance) can be classified into one of the four categories shown in Figure 2:

(a) $P_c > P_m$; $dP/dt > 0$; $\Delta\omega_c > 0$ — i.e. point C lies on the left part of the power-angle characteristic above the mechanical power (Figure 2a).

(b) $P_c > P_m$; $dP/dt < 0$; $\Delta\omega_c > 0$ — i.e. point C lies on the right part of the power-angle characteristic above the mechanical power (Figure 2b).

(c) $P_c < P_m$; $dP/dt > 0$; $\Delta\omega_c > 0$ — i.e. point C lies on the left part of the power-angle characteristic but below the mechanical power (Figure 2c). This is the case when the fault clearance significantly reduces the magnitude of the power-angle characteristic.

(d) $P_c < P_m$; $dP/dt < 0$; $\Delta\omega_c > 0$ — i.e. point C lies on the right part of the power-angle characteristic but below the mechanical power (Figure 2d).

In case (d), the generators lose synchronism during the fault and are switched off by the pole-slip protection. Therefore, this case is not considered further.

In cases (a), (b), and (c), the angles δ_s and δ_u may be calculated based on the active power and the magnitude of the power-angle characteristic:

$$\delta_s = \arcsin(P_m/P_{max}) \quad \text{and } \delta_u = (\pi - \delta_s) \tag{15}$$

The formulas used for calculating angle δ_c and deceleration area A_d differ between individual cases as described below.

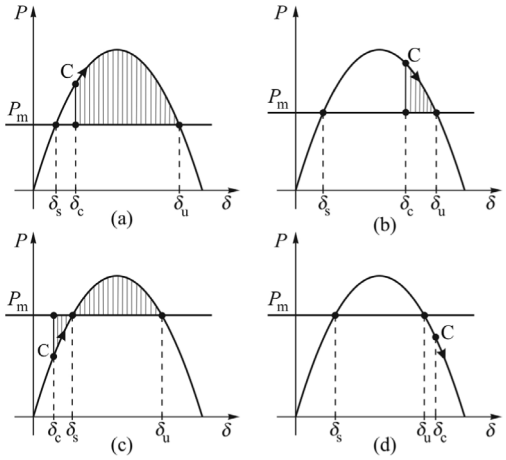

FIGURE 2. Illustration of four possible post-fault states.

Case (a): Figure 2a

Point C lies on the left part of the characteristic $\delta_c < \pi/2$ and

$$\delta_c = \arcsin(P_c/P_{max}) \tag{16}$$

For $\delta_u = (\pi - \delta_s)$, it yields that $\cos(\pi - \delta_s) = -\cos\delta_s$, and from equation (12), the following is obtained:

$$A_d = P_{max}(\cos\delta_c + \cos\delta_s) - P_m(\pi - \delta_s - \delta_c) \tag{17}$$

where $\cos\delta_c > 0$.

Case (b): Figure 2b

Point C lies on the right part of the characteristic $\delta_c > \pi/2$:

$$\delta_c = \pi - \arcsin(P_c/P_{max}) \tag{18}$$

The available deceleration area can also be calculated from the equation (17), but it is much smaller than in case (a) due to the fact that now $\cos\delta_c < 0$.

Case (c): Figure 2c

As shown in the figure, in this case the available deceleration area lies between points δ_s and $\delta_u = (\pi - \delta_s)$. Considering that $\cos\delta_u = -\cos\delta_s$, the following is obtained:

$$\begin{aligned} A_d &= \int_{\delta_s}^{\delta_u} P_{max}\sin\delta d\delta - P_m(\delta_u - \delta_s) \\ &= 2P_{max}\cos\delta_s - P_m(\pi - 2\delta_s) \end{aligned} \tag{19}$$

Moreover, in this case (Figure 2c), after the fault clearance from point C to mechanical power P_m, the generator rotor is accelerated, which increases the kinetic energy:

$$\Delta_a = P_m(\delta_s - \delta_c) - \int_{\delta_c}^{\delta_s} P_{max}\sin\delta d\delta \tag{20}$$

The resultant acceleration area is equal to the sum of the right sides of equations (11) and (20):

$$A_a = \frac{1}{2}M\cdot\Delta\omega_c^2 + P_m(\delta_s - \delta_c) - P_{max}(\cos\delta_c - \cos\delta_s) \tag{21}$$

where δ_s and δ_c are given by equations (15) and (16) respectively.

When stability condition (13) is not met it is necessary to compute the number of generators that must be tripped to preserve the synchronism of the remaining generators.

V. IMPACT OF GENERATOR TRIPPING

A. MAGNITUDE OF POWER-ANGLE CHARACTERISTIC

Tripping some generators can change the mechanical power and the magnitude of the power-angle characteristic. In Figure 3 power-angle characteristics for the state before generator tripping are shown with dashed curves and the characteristics for the state after generator tripping are marked with solid curves. The deceleration areas available after generator tripping are hatched with sloping lines. These areas are larger than those in Figure 2a and b.

Generator tripping reduces the mechanical power of the equivalent generating unit:

$$P_{mR} = P_m - \Delta P_m = r_{Pm}\cdot P_m \quad \text{and } r_{Pm} = 1 - \frac{\Delta P_m}{P_m} \tag{22}$$

$$P_m = \sum_{i=1}^{n} P_{mi} \quad \text{and } \Delta P_m = \sum_{i=1}^{k} P_{mi} \tag{23}$$

where r_{Pm} is the reduction coefficient. P_m is the mechanical power of the equivalent generating unit and ΔP_m is the mechanical power of tripped generating units.

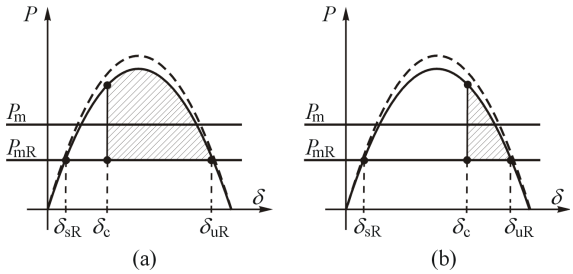

FIGURE 3. Illustration of the impact of generator tripping.

In particular case when powers of all generating units in the given group are equal, the reduction coefficient is:

$$r_{Pm} = 1 - \frac{k}{n} = \frac{n-k}{n} \tag{24}$$

where n is the initial (pre-fault) number of generating unit in the group, and k is the number of tripped generating units.

In addition, generator tripping reduces the magnitude of the power-angle characteristic because (as shown by the circuit diagram in Figure 1) it increases the equivalent reactance to the following value:

$$X_{GR} = X_G\cdot\frac{n}{n-k} = \frac{X_G}{r_{Pm}} \tag{25}$$

The magnitude of the power-angle characteristic is inversely proportional to the equivalent reactance, and therefore:

$$\frac{P_{maxR}}{P_{max}} = \frac{X_G + X_S}{X_{GR} + X_S} \tag{26}$$

Assuming that $\kappa_X = X_S/X_G$ is the ratio between the equivalent reactance of the given group of generators and the equivalent reactance of the system, it is finally obtained from equations (26) and (25) that:

$$P_{maxR} = r_{Pmax} \cdot P_{max}; \quad r_{Pmax} = r_{Pm} \cdot \frac{1 + \kappa_X}{1 + r_{Pm} \cdot \kappa_X} \tag{27}$$

where r_{Pmax} is the reduction coefficient of the power-angle characteristic magnitude.

The values of κ_X may be estimated from the short-circuit power of the system S_K calculated without the considered group of generators and the parameters of these generators:

$$X_S = V_n^2/S_K \quad \text{and } X_G = X_{G(pu)} V_n^2/P_n \tag{28}$$

where V_n is the voltage rating and P_n is the power rating of the considered group of generators, and $X_{G(pu)}$ is the sum of the generator and step-up transformer reactance in pu. From the equation (28), the following can be obtained:

$$\kappa_X = \frac{X_S}{X_G} = \frac{P_n}{S_K} \cdot \frac{1}{X_{G(pu)}} \tag{29}$$

Typical values of S_K/P_n yield $r_{Pmax} < r_{Pm}$. Moreover, for a given value of r_{Pm} coefficient, r_{Pmax} is smaller for the larger values of S_K/P_n. For this reason, when the analysis is performed for a prefault state (N–m) with outage of m network elements, it is not advisable to calculate κ_X using the value of S_K for the state (N-0) as this could lead to the overestimation of the number of the generators to be tripped. Thus, appropriate values of S_K together with other parameters should be memorized in SPS.

B. DETERMINATION OF THE NUMBER OF GENERATORS TO BE TRIPPED

As shown in Figure 3 when mechanical power of the equivalent generating unit is reduced, the stable and unstable equilibrium points δ_{sR} and δ_{uR} move left and right respectively, and have the following coordinates:

$$\delta_{sR} = \arcsin(P_{mR}/P_{maxR}) \quad \text{and } \delta_{uR} = (\pi - \delta_{sR}) \tag{30}$$

For cases (a) and (b) described in Section IV.B, the deceleration area can be calculated from the following formula, which is similar to the formula (17):

$$A_{dR} = P_{maxR} \cdot (\cos\delta_c + \cos\delta_{sR}) - P_{mR} \cdot (\pi - \delta_{sR} - \delta_c) \tag{31}$$

wherein for case (a), the value of δ_c is calculated from the equation (16) and for case (b) from the equation (18).

For case (c), the deceleration area can be calculated from the following formula, which is similar to the formula (19):

$$A_{dR} \cong 2P_{maxR} \cdot \cos\delta_{sR} - P_{mR} \cdot (\pi - 2\delta_{sR}) \tag{32}$$

Reduction of the number of generators also reduces the kinetic energy in the system:

$$A_{aR} = r_{Pm} \cdot A_a \tag{33}$$

In the state with a reduced number of generators, the transient stability margin may be calculated from the formula:

$$K_R = \frac{A_{dR} - A_{aR}}{A_{dR}} \tag{34}$$

Computations of A_{aR} and A_{dR} can be performed consecutively for subsequent values of k ($k = 1, 2 \ldots$) until a value at which the required transient stability margin K_R is obtained. Such a value of k determines the number of generators that must be tripped.

VI. MEASUREMENT ASPECTS

As it is evident from the formulas (8) and (10), for predicting P_{max}, the generator terminal values (Fig. 1) P, Q, V_G should be measured. Many contemporary control systems use digital algorithms decomposing measured voltage and current into orthogonal components: $\underline{I}_G = I_{Gc} + jI_{Gs}$ and $\underline{V}_G = V_{Gc} + jV_{Gs}$, where j is the angular shift by $\pi/2$ and $\underline{I}_G$ and $\underline{V}_G$ are phasors of electrical current and voltage, respectively. The components of each phasor are calculated based on the measurement of samples in the window with a set width. The general formulas used for calculating phasors have been described in many publications, and among others, in the book [1] (Chapter 16).

Using the components of voltage and current phasors, it is possible to calculate: $V_G = |\underline{V}_G|$, $P = V_{Gc}I_{Gc} + V_{Gs}I_{Gs}$, and $Q = V_{Gs}I_{Gc} - V_{Gc}I_{Gs}$.

All switching operations in AC networks involve step changes fast transients in electrical currents and voltage. Therefore, the width of the measurement window should be at least equal to the full cycle of the fundamental frequency in order to measure the abovementioned phasors properly. Such an algorithm washes out the DC component and harmonics. The time of dynamic response to a step change is equal to one cycle of the fundamental frequency. Hence, prediction of P_{max} based on the formulas (8) and (10) should be initiated at least one cycle (i.e. $\Delta t_m = 20$ ms for 50-Hz systems) after fault clearance.

The initiation procedure can be realized using output signals from protections and auxiliary contacts of the circuit breaker. The procedure can be augmented by recognizing a sudden change in reactive power as described in [27].

Derivatives dP/dt and dE/dt can be computed using the Euler method:

$$\left.\frac{dP}{dt}\right|_i = \frac{P_i - P_{i-1}}{t_i - t_{i-1}}; \quad \left.\frac{dE}{dt}\right|_i = \frac{E_i - E_{i-1}}{t_i - t_{i-1}} \tag{35}$$

where i denotes a consecutive step of the sampling period. For example, when sampling frequency is 1000 Hz, the sampling period Δt_s is only 1 ms.

VII. ALGORITHM

The flowchart of the algorithm of the proposed method is shown in Figure 4. The two initial blocks refer to measurements and initiation of the procedure based on the signals from protections and auxiliary contacts of circuit breakers.

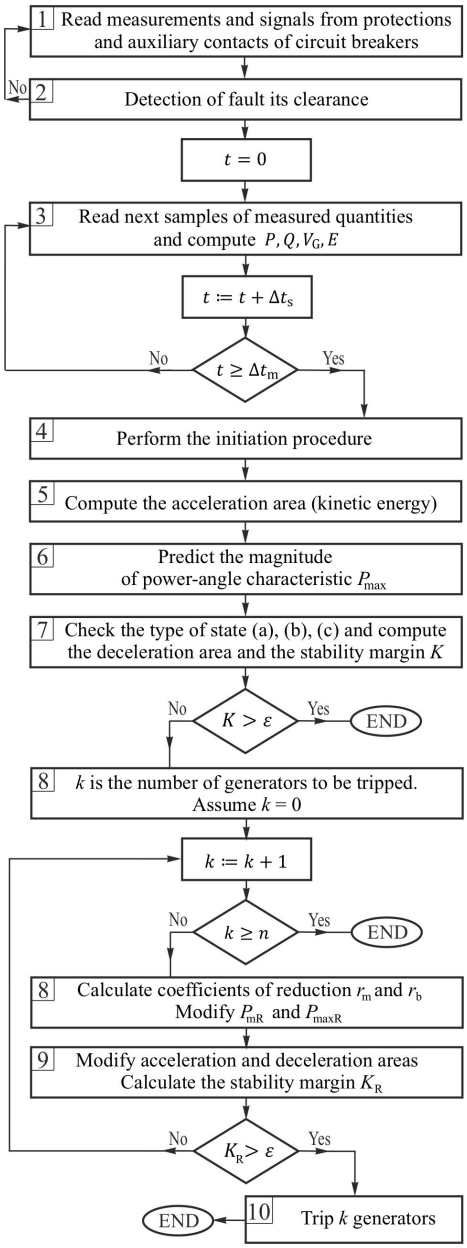

FIGURE 4. Flowchart of the algorithm of the proposed method.

In the third block, full-cycle algorithm and consecutive samples are used to calculate P, Q, V_G, E, later used for prediction. The calculated values are transferred to the subsequent blocks which conduct the prediction process only after time Δt_m.

All calculations related to the magnitude of the power-angle characteristic and instability prediction are performed in the fourth, fifth and sixth blocks where the transient stability margin K is also computed. The procedure is stopped if $K > \varepsilon$, where $\varepsilon > 0$ is a prescribed value of the stability margin. If $K \leq \varepsilon$, then it is necessary to calculate the number of generators that must be tripped. The relevant calculations in the eighth and ninth blocks are performed in the loop. The tripping signal is generated for the smallest value of $k < n$, for which $K_R > \varepsilon$. If for $k = n$ the stability margin K_R is negative or less than ε, the procedure does not generate any tripping signal, because in such situation the given group of generators must be switched off by pole-slip protection.

It is worth recalling here that the formula (24) for reduction coefficient r_{Pm} is valid only when all generating units in the considered group have the same power. When generating units have different powers, r_{Pm} must be calculated based on the formula defined in (22) and the loop with the seventh and eighth blocks (Figure 4) should be performed in a different way, searching for generating units with the smallest power for which $K_R > \varepsilon$.

In the described algorithm, the time required to switch off the selected generators consists of the following components:

(i) Time required to measure P, Q, V_G taking into account the dynamic response of filters and measurement algorithm. In Section VI, this component is estimated as one cycle of the fundamental frequency (i.e. $\Delta t_m = 20$ ms for 50-Hz systems).

(ii) Time required to perform arithmetic operations for calculating P_{max}, predicting instability and estimating the number of tripped generators. For contemporary digital processors used for digital protection and control systems, this component is negligible because such processors perform about 200 numerical instructions in 1 μs.

(iii) Opening time of circuit breakers, which is about two cycles of the fundamental frequency (i.e. $\Delta t_{CB} = 40$ ms for 50-Hz systems).

Hence, the cumulative delay in tripping the selected generating units is approximately estimated as equal to three cycles (i.e. $\Delta t = \Delta t_m + \Delta t_{CB} = 60$ ms for 50-Hz systems).

According to simulation studies, such a small delay does not need be considered when calculating the number of generators to be tripped.

VIII. SIMULATION TESTS

A. TEST SYSTEM

Simulation tests were performed for a real-life power system with a capacity of 28,900 MW, which is a subsystem of a large-scale interconnected power system with a capacity of 166,700 MW. A model of such an interconnected system includes 5883 buses, 6860 lines, 939 transformers, 50 shunt compensators, and 629 synchronous generators. The data of this system can be downloaded from an earlier report [28].

B. CONSIDERED POWER PLANT AND SUBSTATION

A fossil fuel power plant is considered to operate at three voltage levels: 400, 220, and 110 kV. The layout of its substation is shown in Figure 5. More than one generation unit is operating at each voltage level.

It should be noted that all fifteen lines L1-L15 shown in Figure 5 connect this substation to other substations of the considered large-scale system, and the whole power

system [28] is taken into account in the simulations described below.

In the simulation tests, the synchronous generators of the considered power plant have been represented by model GENROU [29]. Exciters of all generators in the considered power plant are of the static type supplied from the generator terminals and have been represented in simulation by model ST1A [30]. Voltage controllers of generators G1–G7 are equipped with the single-input stabilizers represented in simulation by model PSS1A [30] with active power as an input signal. For generators G8–G11, the dual input stabilizers are used, which have been represented in the simulation by model PSS2A [30] with speed deviation and active power as input signals. All steam turbines in the considered power plant have been represented in the simulation by model TGOV3 [31].

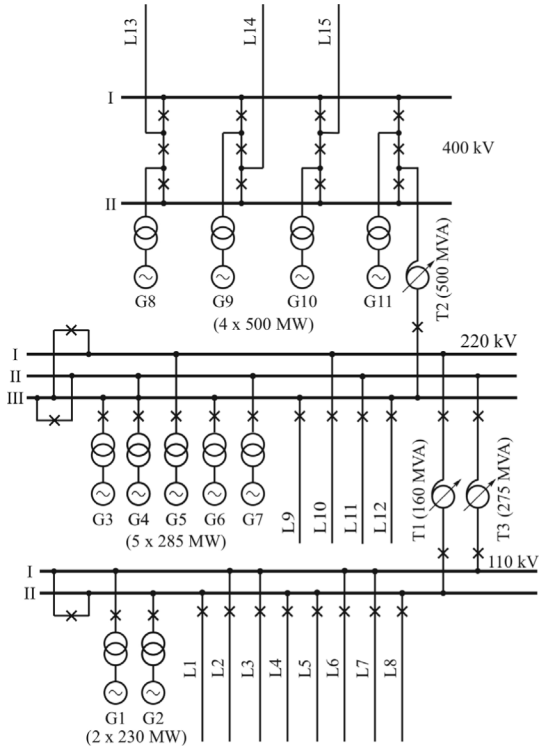

FIGURE 5. Substation layout of the considered power plant, x circuit breaker in the closed position.

Computer simulations have been performed for all types of credible and extreme contingency events described in [1]. In the normal state (N-0), the considered power system is stable with the required transient stability margin. A risk of transient instability or of events with insufficient stability margin has been recognized in the state (N-1) with the outage of transformer T2. For generators G3–G7, transformer T2 makes an important connection with the transmission network 400 kV (Figure 5). In this state, the three-phase faults in the transmission lines 220 kV near the busbars may lead to the loss of synchronism of generators G3–G7. The performance of the proposed prediction method is illustrated by some examples below.

C. PREDICTION OF POWER-ANGLE CHARACTERISTIC MAGNITUDE

In the three examples given, an outage of transformer T2 is assumed in the initial state and the faults are located in the transmission network 220 kV near the busbars of the considered substation (Figure 5).

It should be noted here that $P_{\max} = EV/X$ is determined by reactance X which contains equivalent network reactance X_S. In the post-fault state, X_S depends on which of the transmission lines were switched off for fault clearance. Therefore, $P_{\max}$ values obtained for various fault locations (e.g. L9, L10, L11) differ.

Moreover, $P_{\max} = EV/X$ is also influenced by transient electromotive force E, which is subject to small, slow changes during synchronous power swings and slightly higher changes during asynchronous operation [1] (Chapter 6.5). However, for instability prediction, the value of $P_{\max} = EV/X$ immediately after fault clearance is relevant.

Example 1: Figure 6 shows the loss of synchronism and asynchronous operation of generators G3–G7 after the three-phase short circuit at the beginning of line L9. The clearing time is $t_c = 120$ ms. The blue solid curve in the figure shows the waveform of the active power $P(t)$ of the equivalent generator representing generators G3–G7.

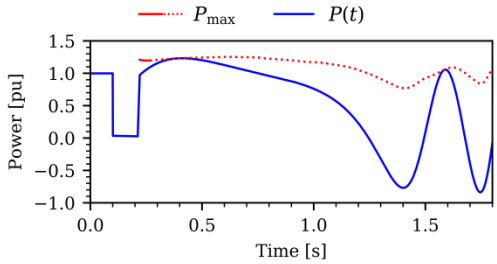

FIGURE 6. The waveforms of active power $P(t)$ and predicted $P_{\max}$ in the case of the asynchronous operation.

The short red curve shown just after the fault clearance indicates the $P_{\max}$ value obtained from the formula (8). The further part depicted by the dotted curve shows the changes in $P_{\max}(t)$ during the asynchronous operation due to changes in the transient electromotive force. As it is known [1], during the asynchronous operation, the magnitudes of the power-angle characteristic $P_{\max}$ are equal to the consecutive peaks of $P(t)$. The short red curve shown in the figure illustrates that immediately after the fault clearance the proposed method predicts the value of $P_{\max}$ properly, which power $P(t)$ reaches about 200 ms later.

Example 2: Figure 7 shows the deep synchronous swings caused by the three-phase short circuit at the beginning of line L10. The clearing time is $t_c = 120$ ms. As in the previous example, the blue solid curve (Figure 7a) shows the waveform of active power $P(t)$ and the short red curve shown just after the fault clearance indicates the $P_{\max}$ value obtained from the formula (8). In this case, during the forward motion, $P(t)$ passes over the peak of the power-angle characteristic

TABLE 1. Example of stability assessment obtained by the proposed method and simulation.

Initial state Outage Ratio	κ_x	Faulted line	Tripped generator	Speed deviation at t_c	Active power at t_c	Mechanical power	Magnitude of power-angle characteristic	Accele-ration area	Decele-ration area	Stability margin	Stability result by simulation
				rad/s	pu	pu	pu	pu·rad	pu·rad	%	-
(N-1) T2 S_K/P_n=2.6	0.855	L9	-	3.779	0.973	0.998	1.252	0.234	0.218	-7.8	No
			G7			0.799	1.103	0.186	0.304	36.7	Yes
		L10	-	3.763	1.009	0.998	1.280	0.225	0.254	11.4	Yes
		L11	-	3.776	1.007	0.998	1.300	0.227	0.281	19.3	Yes
		L12	-	3.795	1.021	0.998	1.260	0.229	0.227	-1.1	No
			G7			0.799	1.110	0.183	0.308	40.5	Yes
(N-2) T2, T1 S_K/P_n=2	1.111	L9	-	3.798	0.940	0.998	1.130	0.244	0.085	-196	No
			G7			0.799	1.010	0.184	0.183	-0.3	No
			G7, G6			0.599	0.859	0.138	0.261	47.2	Yes

and then decreases along its right part. During the backward motion, the power increases and again passes over the peak of the power-angle characteristic. For this reason, after the fault clearance, the waveform $P(t)$ has two characteristic humps which disappear later when the oscillations are damped out. Figure 7b shows the same curves but for a shorter time. This enlarged figure shows better that soon after the fault clearance the proposed method predicts the value of $P_{\max}$ properly, which power $P(t)$ reaches about 200 ms later.

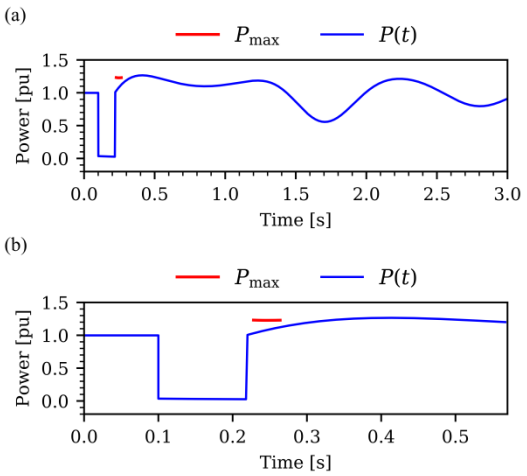

FIGURE 7. The waveforms of active power $P(t)$ and predicted $P_{\max}$ in the case of deep synchronous swings.

Example 3: Figure 8 shows the small synchronous swings caused by the three-phase temporary short circuit at busbars 220 kV. The clearing time is $t_c = 80$ ms. In this case, the waveform $P(t)$ does not reach the peak of the power-angle characteristic. However, immediately after the fault is cleared, the proposed method properly predicts the value of $P_{\max}$, which in Figure 8a and b is depicted by a short red curve.

D. PREDICTION OF INSTABILITY AND NUMBER OF TRIPPED GENERATORS

The examples of the results obtained by the proposed method and simulation are presented in Table 1. In all cases, it is

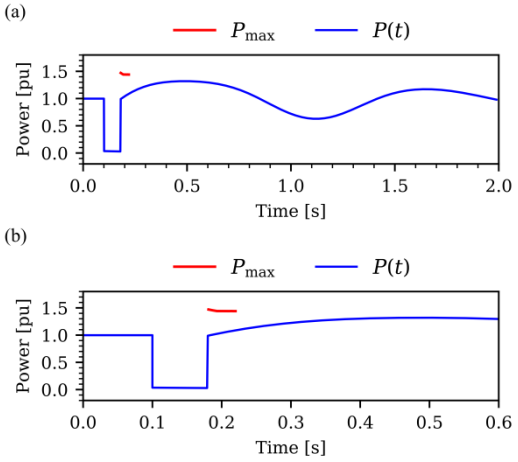

FIGURE 8. The waveforms of active power $P(t)$ and predicted $P_{\max}$ in the case of small synchronous swings.

assumed that the three-phase fault occurs at the beginning of the line and the clearing time is $t_c = 120$ ms.

The simulation results obtained for the first case listed in Table 1 (outage of T2 and short circuit in line L9) are shown in Figure 6. The considered group of generators loses synchronism about 500 ms after the fault clearance. The proposed method predicts this impending event just after the fault clearance. Moreover, it also predicts correctly that tripping only one generator will preserve the synchronism, which is confirmed by Figure 9. The blue solid curve in this figure shows the synchronous power swing, when one generator is tripped with a delay $\Delta t = 60$ ms mentioned in Section VI. The dotted curve shows the waveform of $P(t)$ in the case without generator tripping.

In the next two cases listed in Table 1 (outage of T2 and short circuit in lines L10 and L11), the proposed method predicts stability correctly.

In the fourth case listed in Table 1 (outage of T2 and short circuit in line L12), the proposed method predicts instability as well as the fact that only one generator must be tripped correctly.

In the last case listed in Table 1 (outage of T2 and T1 and short circuit in line L9), the proposed method predicts the

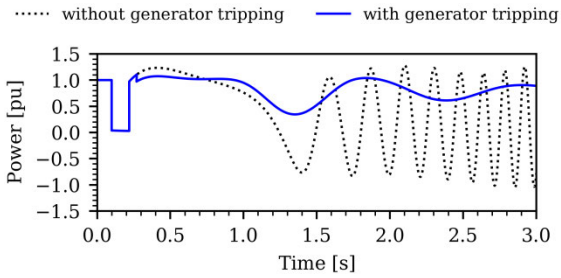

FIGURE 9. The waveforms of active power $P(t)$ in the case without and with generator tripping.

impending instability as well as the fact that two generators must be tripped to preserve synchronism correctly. The simulation (analogous to Figure 9) also confirmed that in this case two generators must be tripped in order to preserve synchronism.

E. UNBALANCED FAULTS

It should be noted that the examples described above are for three-phase faults. Simulation tests have been also performed for unbalanced faults (phase to phase and phase to ground). The proposed method and simulations have demonstrated that the considered system is stable for such faults.

IX. CONCLUSION

This paper presents a new method which enables quick real-time prediction of transient instability and the number of generators that must be tripped to preserve the synchronism of the remaining generators. This method is founded on predicting the magnitude of power-angle characteristic. Some significant advantages of the proposed method are as follows:

- only locally measurable signals available in the considered substation are used,
- the prediction requires performing only simple mathematical operations, which reduces the time needed to generate the tripping signal,
- the method allows to assess the magnitude of power-angle characteristic just after the fault clearance for normal as well as for extreme contingency events.

Simulation tests for a large-scale real power system using detailed models of power system elements have confirmed the validity and robustness of the proposed method.

REFERENCES

[1] J. Machowski, Z. Lubosny, J. Bialek, and J. Bumby, *Power System Dynamics. Stability and Control*, 3rd ed. New York, NY, USA: Wiley, 2020.

[2] NERC North American Electric Reliability Corporation, *Reliability Standards for the Bulk Electric Systems in North America*. Standard TPL-001-2, Transmission System Planning Performance Requirements, 2011. Accessed: Apr. 17, 2019. [Online]. Available: http://www.nerc.com

[3] P. Kundur, *Power System Stability and Control*. New York, NY, USA: McGraw-Hill, 1994.

[4] *Defense Plan Against Extreme Contingencies*, CIGRE, Paris, France, Tech. Brochure no. 316, 2007.

[5] *A Proposed Framework for Coordinated Power System Stability Control*, CIGRE, Paris, France, Tech. Brochure no. 742, 2018.

[6] Y. Cong, P. Regulski, P. Wall, M. Osborne, and V. Terzija, "On the use of dynamic thermal-line ratings for improving operational tripping schemes," *IEEE Trans. Power Del.*, vol. 31, no. 4, pp. 1891–1900, Aug. 2016, doi: 10.1109/TPWRD.2015.2502999.

[7] S. Robak, J. Machowski, and K. Gryszpanowicz, "Automatic alleviation of overloads in transmission network by generation curtailment," *IEEE Trans. Power Syst.*, vol. 33, no. 4, pp. 4424–4432, Jul. 2018, doi: 10.1109/TPWRS.2017.2775799.

[8] *Determining Generator Fault Clearing Time for the Synchronous Zone of Continental Europe, ENTSO-E, Version 1.0 - RG-CE System Protection & Dynamics Sub Group*. Accessed: Feb. 3, 2017. [Online]. Available: https://eepublicdownloads.entsoe.eu/clean-documents/SOC%20documents/Regional_Groups_Continental_Europe/2017/SPD_FCT-BestPractices_website.pdf

[9] *NERC/WECC Planning Standards-Special Protection Systems (SPS)/Remedial Action Schemes (RAS): Assessment of Definition, Regional Practices, and Application of Related Standards*. Accessed: Sep. 10, 2012. [Online]. Available: https://www.NERC.com

[10] C. A. Stigers, C. S. Woods, J. R. Smith, and R. D. Setterstrom, "The acceleration trend relay for generator stabilization at Colstrip," *IEEE Trans. Power Del.*, vol. 12, no. 3, pp. 1074–1081, Jul. 1997, doi: 10.1109/61.636872.

[11] G. G. Karady and J. Gu, "A hybrid method for generator tripping," *IEEE Trans. Power Syst.*, vol. 17, no. 4, pp. 1102–1107, Nov. 2002, doi: 10.1109/TPWRS.2002.805014.

[12] G. G. Karady, "Improving transient stability using generator tripping based on tracking rotor-angle," in *Proc. IEEE Power Eng. Soc. Winter Meeting. Conf.*, Jan. 2002, pp. 1113–1118.

[13] A. R. Sobbouhi and A. Vahedi, "Transient stability prediction of power system: A review on methods, classification and considerations," *Electr. Power Syst. Res.*, vol. 190, Jan. 2021, Art. no. 106853, doi: 10.1016/j.epsr.2020.106853.

[14] M. Pertl, T. Weckesser, M. Rezkalla, and M. Marinelli, "Transient stability improvement: A review and comparison of conventional and renewable-based techniques for preventive and emergency control," *Electr. Eng.*, vol. 100, no. 3, pp. 1701–1718, Sep. 2018, doi: 10.1007/s00202-017-0648-6.

[15] X. Xu, H. Zhang, C. Li, Y. Liu, W. Li, and V. Terzija, "Optimization of the event-driven emergency load-shedding considering transient security and stability constraints," *IEEE Trans. Power Syst.*, vol. 32, no. 4, pp. 2581–2592, Jul. 2017.

[16] *Wide Area Protection & Control Technologies*, CIGRE, Paris, France, Tech. Brochure no. 664, 2016.

[17] X. Wu, A. Xu, J. Zhao, H. Deng, and P. Xu, "Review on transient stability prediction methods based on real time wide-area phasor measurements," in *Proc. 4th Int. Conf. Electric Utility Deregulation Restructuring Power Technol. (DRPT)*, Weihai, Shandong, Jul. 2011, pp. 320–326, doi: 10.1109/DRPT.2011.5993910.

[18] D. Min, S.-J. Kim, S. Seo, Y.-H. Moon, K. Sun, J. H. Chow, and K. Hur, "Computing safety margins of a generation rejection scheme: A framework for online implementation," *IEEE Trans. Smart Grid*, vol. 9, no. 3, pp. 2337–2346, May 2018, doi: 10.1109/TSG.2016.2635687.

[19] H. Supreme, L.-A. Dessaint, I. Kamwa, and A. Heniche-Oussedik, "Development of new predictors based on the concept of center of power for transient and dynamic instability detection," *IEEE Trans. Smart Grid*, vol. 9, no. 4, pp. 3605–3615, Jul. 2018, doi: 10.1109/TSG.2016.2636816.

[20] A. Paul, I. Kamwa, and G. Joos, "PMU signals responses-based RAS for instability mitigation through on–the fly identification and shedding of the run-away generators," *IEEE Trans. Power Syst.*, vol. 35, no. 3, pp. 1707–1717, May 2020, doi: 10.1109/TPWRS.2019.2926243.

[21] G. C. Zweigle and V. M. Venkatasubramanian, "Transient instability mitigation for complex contingencies with computationally constrained cost-based control," *IEEE Trans. Smart Grid*, vol. 7, no. 4, pp. 1961–1969, Jul. 2016.

[22] S. K. Azman, Y. J. Isbeih, M. S. E. Moursi, and K. Elbassioni, "A unified online deep learning prediction model for small signal and transient stability," *IEEE Trans. Power Syst.*, vol. 35, no. 6, pp. 4585–4598, Nov. 2020, doi: 10.1109/TPWRS.2020.2999102.

[23] M. Pavella, D. Ernst, and D. Ruiz-Vega, *Transient Stability of Power Systems: A Unified Approach to Assessment and Control*. Norwell, MA, USA: Kluwer, 2000.

[24] Y. Xue, T. Van Custem, and M. Ribbens-Pavella, "Extended equal area criterion justifications, generalizations, applications," *IEEE Trans. Power Syst.*, vol. 4, no. 1, pp. 44–52, Feb. 1989.

[25] S.-C. Oh, H.-I. Lee, Y.-H. Lee, and B.-J. Lee, "A novel SIME configuration scheme correlating generator tripping for transient stability assessment," *J. Elect. Eng. Technol.*, vol. 13, no. 5, pp. 1798–1806, 2018. [Online]. Available: http://doi.org/10.5370/JEET.2018.13.5.1798
[26] Y. Xue, X. Zhu, and Z. Li, "Influence of generator-tripping time on transient stability," in *Proc. IEEE Innov. Smart Grid Technol.-Asia (ISGT Asia)*, Chengdu, China, May 2019, pp. 916–921, doi: 10.1109/ISGT-Asia.2019.8881302.
[27] R. Kobayashi, K. Maekawa, K. Shimomura, T. Sasaki, Y. Kowada, and T. Maeda, "Development of sequential calculating type autonomous stabilizing controller for maintaining transient stability in case of backup relay operation in load system," *IEEE Trans. Power Syst.*, vol. 26, no. 3, pp. 1317–1325, Aug. 2011, doi: 10.1109/TPWRS.2010.2090673.
[28] *ENTSO-E Initial Dynamic Model of Continental Europe*. Accessed: Apr. 24, 2020. [Online]. Available: https://www.entsoe.eu/publications/system-operations-reports/#entso-e-dynamic-model-of-continental-europe
[29] J. Weber. *Description of Machine Models GENROU, GENSAL, GENTPF and GENTPJ*. Power World Corporation. Accessed: Dec. 3, 2015. [Online]. Available: https://www.powerworld.com/files/GENROU-GENSAL-GENTPF-GENTPJ.pdf
[30] *IEEE Recommended Practice for Excitation System Models for Powers System Stability Studies*, IEEE Power Engineering Society, IEEE Standard 421.5-2016, 2016.
[31] I. Power and E. Society, "Dynamic models for turbine-governors in power system studies," PES-TR1 prepared by Power Syst. Dyn. Perform. Committee, Power Syst. Stability Subcommittee, Task Force Turbine-Governor Model., IEEE Power Energy Soc., Tech. Rep. PES-TR1, Jan. 2013. [Online]. Available: https://site.ieee.org/fw-pes/files/2013/01/PES_TR1.pdf

SYLWESTER ROBAK (Member, IEEE) received the M.Sc., Ph.D., and D.Sc. degrees in electrical engineering from the Faculty of Electrical Engineering, Warsaw University of Technology (WUT), Poland, 1996, 1999, and 2008, respectively. He has been associated with Warsaw University of Technology, since 1999. From 2008 to 2012, he was the Deputy Director of the Electrical Power Engineering Institute, WUT. From 2012 to 2016, he was the Vice-Dean of the Faculty of Electrical Engineering, WUT. His research interests include power system stability and control.

JAN MACHOWSKI (Member, IEEE) received the M.Sc., Ph.D., and D.Sc. degrees from the Faculty of Electrical Engineering, Warsaw University of Technology (WUT), Poland, 1974, 1978, and 1982, respectively. Since 1978, he has been working with WUT. From 1989 to 1992, he was a Visiting Professor at Kaiserslautern University. Since 1993, he has been a Full Professor at Warsaw University of Technology. He is a coauthor of a textbook *Power System Dynamics: Stability and Control* (Wiley & Sons), in 1997, 2008, and 2020. His research interests include power systems analysis, control, and protection.

MATEUSZ M. SKWARSKI was born in Nidzica, Poland, in 1993. He received the B.Sc. (Hons.) and M.Sc. degrees in electrical engineering from the Faculty of Electrical Engineering, Warsaw University of Technology (WUT), Poland, 2017 and 2018, respectively. He is currently pursuing the Ph.D. degree with the Electrical Power Engineering Institute, WUT. His research interests include power systems and especially power system stability analysis. Since 2018, he has been employed at the Research and Development Centre, PSE Innowacje sp. z o.o.

ADAM SMOLARCZYK received the Ph.D. and D.Sc. degrees from the Faculty of Electrical Engineering, Warsaw University of Technology (WUT), Poland, in 1999 and 2020, respectively. Since 1999, he has been working with WUT as an Assistant Professor. He is an author and coauthor of research reports on digital power relays. His research interests include digital power protection automatics and the modeling of phenomena occurring in power systems.